GEOPHYSICS

The slow earthquake spectrum in the Japan Trench illuminated by the S-net seafloor observatories

T. Nishikawa[1]*, T. Matsuzawa[2], K. Ohta[1], N. Uchida[3], T. Nishimura[1], S. Ide[4]

Investigating slow earthquake activity in subduction zones provides insight into the slip behavior of megathrusts, which can provide important clues about the rupture extent of future great earthquakes. Using the S-net ocean-bottom seismograph network along the Japan Trench, we mapped a detailed distribution of tectonic tremors, which coincided with very-low-frequency earthquakes and a slow slip event. Compiling these and other related observations, including repeating earthquakes and earthquake swarms, we found that the slow earthquake distribution is complementary to the Tohoku-Oki earthquake rupture. We used our observations to divide the megathrust in the Japan Trench into three along-strike segments characterized by different slip behaviors. We found that the rupture of the Tohoku-Oki earthquake, which nucleated in the central segment, was terminated by the two adjacent segments.

Slow earthquakes are fault slip phenomena that occur over longer time scales than ordinary earthquakes with comparable seismic moment (*1*). Slow earthquakes include low-frequency earthquakes (LFEs); tectonic tremors, which are swarms of LFEs; very-low-frequency earthquakes (VLFs); and slow slip events (SSEs). Observations of slow earthquakes occur at time scales ranging from a fraction of a second to years. Because slow earthquakes occur in the vicinity of megathrust earthquakes, the slow and fast shear deformations of these different earthquakes interact. Increasingly, observations suggest that slow earthquakes sometimes precede megathrust earthquakes, such as the 2011 M_w 9.0 Tohoku-Oki (*2*, *3*) and 2014 M_w 8.1 Iquique (*4*) earthquakes. Slow earthquakes are also related to the rupture termination of megathrust earthquakes. Areas hosting frequent SSEs impeded the rupture propagation of the 2012 M_w 7.6 Costa Rica (*5*) and 2016 M_w 7.8 Pedernales Ecuador (*6*) earthquakes. Elucidating the entire spectrum of slow earthquake activity on megathrusts may therefore help us to infer the occurrence time and rupture extent of future megathrust earthquakes.

The Japan Trench is a subduction zone off the northeast region of the main island of Japan, where the Pacific Plate subducts under the Okhotsk Plate. The 2011 M_w 9.0 Tohoku-Oki earthquake, which is the largest megathrust earthquake recorded in Japan, ruptured the plate interface of this subduction zone. In the Japan Trench, VLFs have been detected using onshore broadband seismometers (*7*), and SSEs and tectonic tremors preceding the Tohoku-Oki earthquake have been inferred from ocean-bottom pressure gauge and seismograph observations (*2*, *3*). Other indicators of aseismic slip are from observations of repetitive ruptures on the same fault patches, called repeating earthquakes ("repeaters") (*8*), and increases in the seismicity rate without a distinguishable mainshock, called earthquake swarms (*9*). Previous studies (*8*–*10*) have reported recurrent SSEs in the Japan Trench based on analyses of repeating earthquakes and earthquake swarms. Despite these efforts, the entire spectrum of slow earthquake activity and its relation to the Tohoku-Oki earthquake remains poorly resolved, and the Japan Trench has been considered "quiet" in terms of slow earthquake activity relative to the well-studied Nankai subduction zone in southwest Japan (*11*).

In 2016, the National Research Institute for Earth Science and Disaster Resilience (NIED) started the operation of the Seafloor Observation Network for Earthquakes and Tsunamis along the Japan Trench (S-net) (*12*, *13*). The S-net consists of 150 seafloor observatories equipped with ocean-bottom seismometers (OBSs) and pressure gauges that are distributed over the Japan Trench and southern end of the Kuril Trench (Fig. 1A). This wide and dense OBS network has enabled near-field observations of tiny tectonic tremor signals near the trench. Quite recently, high tectonic tremor activities to the north of 39.6°N and at approximately 36.7°N in the Japan Trench were reported by the S-net and temporal OBS observations, respectively (*14*, *15*). However, overall tectonic tremor activity from 34.6°N to 39.6°N, which is ~600 km along the trench, is still unclear. In this study, we used the S-net seismograms and other seismological and geodetic observations to map a detailed spatial distribution of various earthquake phenomena (i.e., tectonic tremors, VLFs, SSEs, repeaters, and earthquake swarms) along the entire Japan Trench. On the basis of the slow earthquake distribution, we investigated the relationship between slow and megathrust earthquakes along the Japan Trench.

We detected tremors along the Japan Trench from continuous S-net OBS seismograms during the 15 August 2016 to 14 August 2018 time period using the envelope correlation method (*16*) within the orange shaded regions in Fig. 1A (*13*). The tremors were distributed to the south of 37°N and to the north of 39°N along the 10- to 20-km depth contours, with only 0.15% of the detected events located in the main rupture area of the 2011 Tohoku-Oki earthquake between 37.3°N and 38.7°N (*17*). Given the almost homogeneous observation conditions of the S-net and the common parameters in the envelope correlation method (*13*), we concluded that the probability of tremor occurrence in this region is substantially smaller than in the northern and southern regions.

The characteristics of these tremors resemble those of deep tremors detected in the Nankai Trough at 30 to 40 km depth (*16*) in terms of waveforms, episodicity, along-strike migration speed, and association with VLFs and SSEs. Similar to deep tremors in Nankai, typical tremor waveforms in the Japan Trench lacked clear *P*- and *S*-wave arrivals and lasted several tens of seconds or longer (Fig. 2). These tremors occurred episodically in clusters (Fig. 1B), as in Nankai (*16*). We observed repeated along-strike tremor migration episodes, each ~1 week long, whose speed ranged from ~10 to 20 km/day between 40.7°N and 42°N (Fig. 1C and fig. S1), where VLFs had also been detected (*18*). This migration speed is also comparable to that of along-strike migration episodes of deep tremors in western Shikoku of Nankai (~5 to 20 km/day) (*16*). Tremors along the Japan Trench were spatially correlated with and sometimes coincided with VLFs located at approximately 40°N and 36.7°N in our VLF catalog (Fig. 1, A and B, and Fig. 2) (*13*). Tremors were not always accompanied by VLFs (Fig. 1B) as in Nankai (*19*). However, tremors without the excitation of VLFs do not preclude a possibility of occurrences of smaller VLFs because of the low signal-to-noise ratio in our VLF detection (*13*). We also observed tremors between 35.2°N and 36.0°N that followed a possible SSE detected by our Global Navigation Satellite System (GNSS) analysis in June 2017 (Fig. 1, A and E) (*13*). This association between an SSE and tremors, called episodic tremor and slip, is also observed in Nankai (*11*). These tremor characteristics common between the Japan Trench and Nankai Trough imply that the high-tremor regions of these two subduction zones share similar frictional properties and fault zone rheology.

By contrast, tremors in the Japan Trench and deep tremors in Nankai are strikingly different with respect to the coincidence of tremors and ordinary interplate earthquakes. The tremors we detected between 39°N and 40.7°N occurred almost simultaneously with $M > 4.5$ ordinary

[1]Disaster Prevention Research Institute, Kyoto University, Uji, Japan. [2]National Research Institute for Earth Science and Disaster Resilience, Tsukuba, Japan. [3]Graduate School of Science and International Research Institute of Disaster Science, Tohoku University, Sendai, Japan. [4]Department of Earth and Planetary Science, University of Tokyo, Tokyo, Japan.
***Corresponding author. Email: nishikawa.tomoaki.68s@st.kyoto-u.ac.jp**

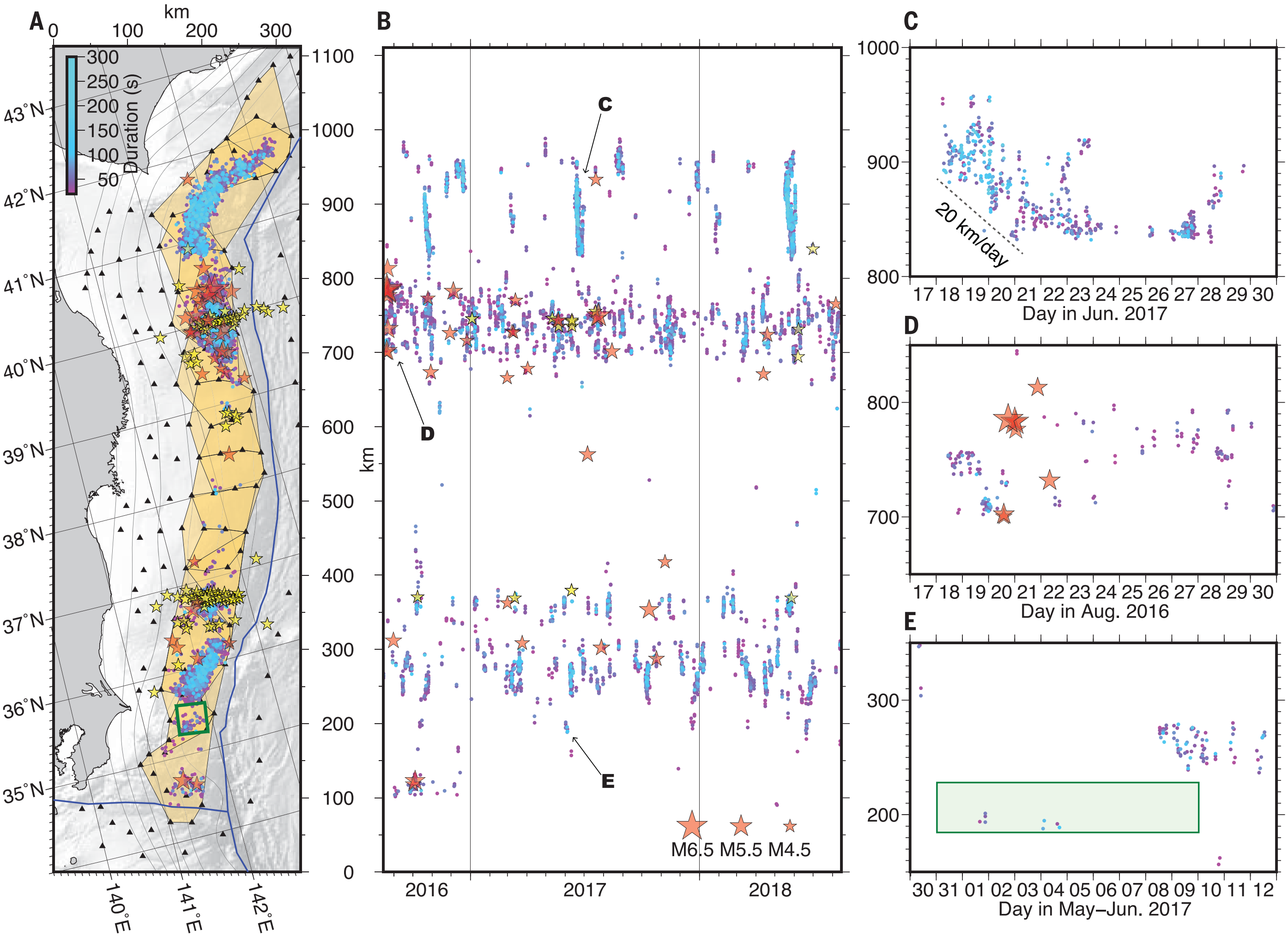

Fig. 1. Tremor activity in the Japan Trench. (**A**) Epicenters of the tectonic tremors. Dots indicate the epicenters of the tremors, which are colored according to their duration (see the color scale). Yellow and red stars are VLFs and $M > 4.5$ ordinary earthquakes, respectively, with the ordinary earthquake epicenters taken from the Japan Meteorological Agency (JMA) catalog. Black triangles are S-net observatories. The green square denotes the June 2017 SSE that was detected by our GNSS analysis. The orange shaded polygons indicate the 18 overlapping subregions used for our tremor detection. The top of the Pacific Plate is indicated by the black contours at 10-km depth intervals. (**B**) Space-time distribution of the tectonic tremors. We used Japanese Standard Time (JST; UTC + 9 hours). The vertical lines indicate 1 January 2017 and 1 January 2018. (**C** to **E**) Enlarged views of (B). The green shaded region in (E) denotes the spatiotemporal extent of the June 2017 SSE.

earthquakes, including some $M \geq 6$ interplate events and their aftershocks (Fig. 1D). This tremor activity was more continuous in time and had a shorter average duration (44 s) than what we detected between 40.7°N and 42°N (64 s; Fig. 1B). In addition, deep tremors in Nankai are distributed more continuously along strike than tremors in the Japan Trench. An along-strike tremor gap longer than 200 km, like the central region of the Japan Trench (37°N to 39°N; Fig. 1A), is not observed for deep tremors in Nankai (*11*).

We compared the epicenters of the tremors, VLFs, and earthquake swarms containing repeaters ($M \geq 3$) to compile slow earthquake–related observations (Fig. 3). We extracted the swarms containing repeaters during the January 1991 to December 2010 and January 2014 to August 2016 time periods from our repeater and swarm catalogs (*13*). We grouped the earthquake swarms into "background swarms," whose first event is a background event, and "aftershock swarms," whose first event is an aftershock of a preceding earthquake (*13*). The background and aftershock swarms containing repeaters are potentially indicative of spontaneous SSEs and afterslip, respectively (*9*, *13*). The relation between earthquake swarms and aseismic slip transients is further discussed in (*13*).

On the basis of Fig. 3, we divided slow earthquake activity in the Japan Trench into three along-strike segments: (i) Ibaraki-Oki (south of 37.3°N), (ii) Miyagi-Oki (37.3°N to 39°N), and (iii) Sanriku-Oki (39°N to 40.7°N). We refer to these as the southern, central, and northern segments, respectively. Tremors, VLFs, and background swarms were concentrated in the southern and northern segments. In particular, most of the background swarms were concentrated at the edge of the large coseismic slip area of the Tohoku-Oki earthquake. The events we detected in the southern segment were primarily located within and around the afterslip area of the Tohoku-Oki earthquake (*20*). Unlike in other subduction zones, tremors and swarms containing repeaters were in close proximity to each other (Fig. 3A and fig. S2). Numerous background swarms suggest the frequent occurrence of spontaneous SSEs in the southern segment. Supporting this inference, our GNSS analysis detected transient displacements of several possible SSEs, one of which accompanied tremors in June 2017 (*13*). In the northern segment, we located tectonic tremors and VLFs around 40°N and 143.6°E (Fig. 3A and fig. S2B). Surrounding these tremors and VLFs, earthquake swarms containing repeaters were distributed around 39.4°N and 143.6°E, and around 40.2°N and 143°E (fig. S2B). These two

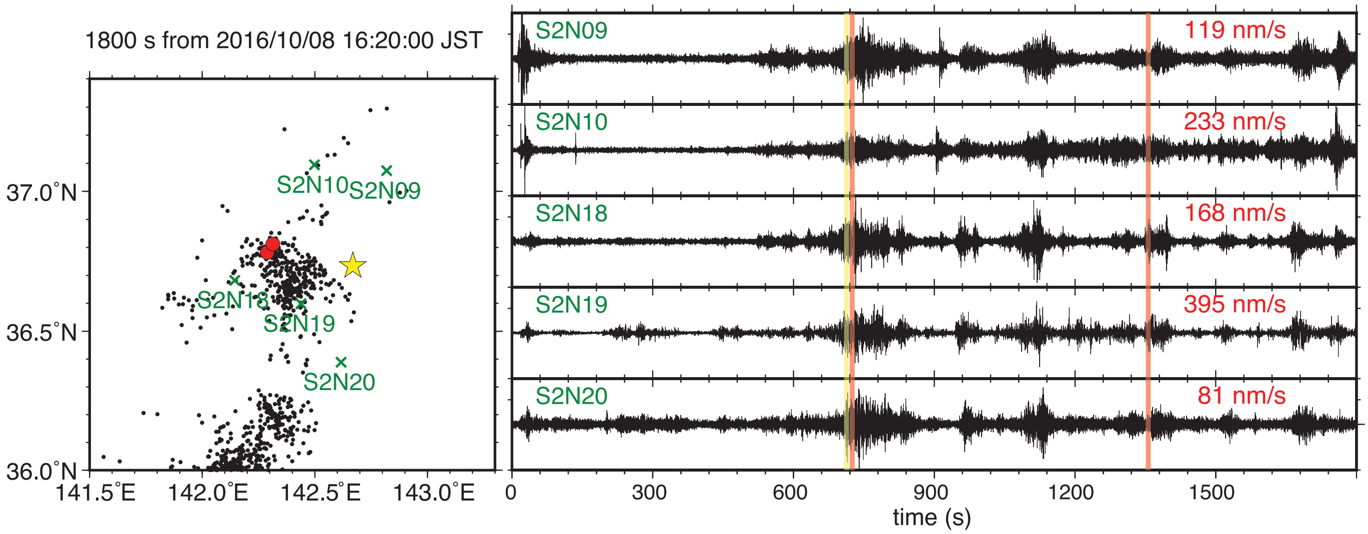

Fig. 2. Waveforms of tectonic tremors coinciding with a VLF. Right: Normalized horizontal seismograms bandpass-filtered at 2 to 8 Hz. The red and yellow vertical lines indicate the origin times of the detected tremors and VLF, respectively. Left: Epicenters of the tremors (red circles), VLF (yellow star), and ocean-bottom observatory locations (green crosses). The black dots denote the other tremors detected in this area.

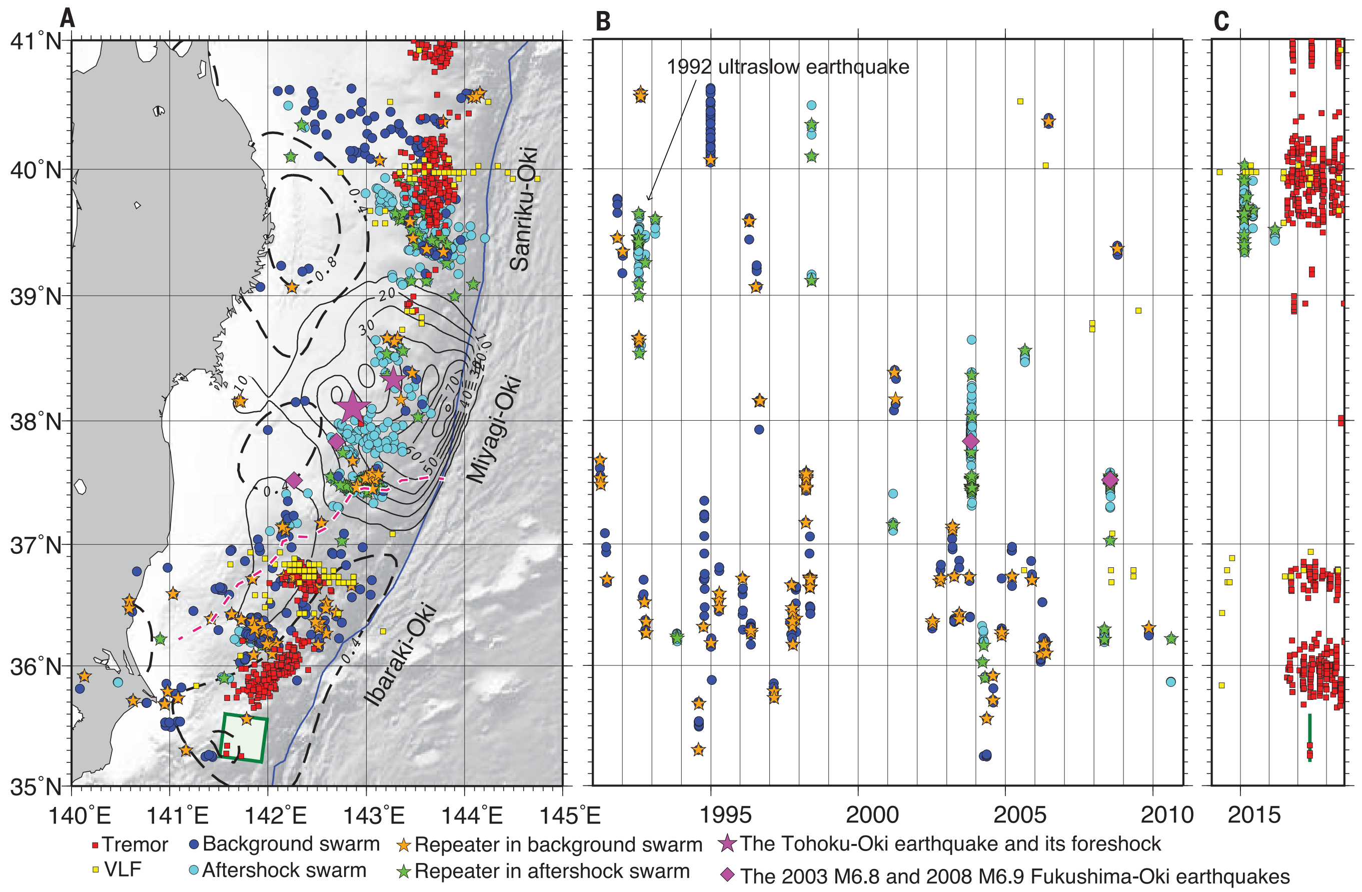

Fig. 3. Slow earthquake activity in the Japan Trench. (**A**) Epicenters of the tectonic tremors, VLFs, and earthquake swarms containing repeaters. Red squares indicate tremors with a duration of 80 s or longer. Yellow squares denote VLFs. Blue circles represent events of background swarms containing repeaters (orange stars). Cyan circles are events of aftershock swarms containing repeaters (green stars). The green square denotes the June 2017 SSE. Magenta diamonds indicate the 2003 *M* 6.8 and 2008 *M* 6.9 Fukushima-Oki earthquakes. Magenta large stars denote the epicenters of the Tohoku-Oki earthquake and its largest foreshock (M_w 7.3). The solid and dashed black contours indicate the coseismic slip (*17*) and afterslip (*20*) distributions of the Tohoku-Oki earthquake at 10-m and 0.4-m intervals, respectively. The magenta dashed line indicates the forearc segment boundary (*24*). (**B** and **C**) Space-time distributions of the tectonic tremors, VLFs, and earthquake swarms containing repeaters during the 1991–2010 and 2014–2018 time periods, respectively.

swarm-prone areas are known to host ~3-year periodic slow slip (*10*). This periodic slow slip includes the 1989 and 1992 "ultraslow earthquakes" (*21*) (Fig. 3B), which were SSEs accompanied by swarms of $M \geq 6$ interplate earthquakes and located at approximately 39.4°N and 143.6°E (*8*, *10*). Furthermore, the section updip of the tremors and ultraslow earthquakes hosted a tsunami earthquake in 1896 (*22*). In contrast, the coseismic rupture area of the Tohoku-Oki earthquake (the central segment) was characterized by fewer tremors, VLFs, and background swarms, but aftershock swarms were detected in this segment. These swarms included aftershocks of the 2003 *M* 6.8 and 2008 *M* 6.9 Fukushima-Oki earthquakes, which suggests that the coseismic rupture area of the Tohoku-Oki earthquake experienced afterslip of these interplate earthquakes. This implies that the large fully coupled region in the central segment, which was inferred from GNSS observations prior to the Tohoku-Oki earthquake (*23*), was eroded by these afterslips. In contrast, the northern and southern segments were only partially coupled (*23*). Consistently, our

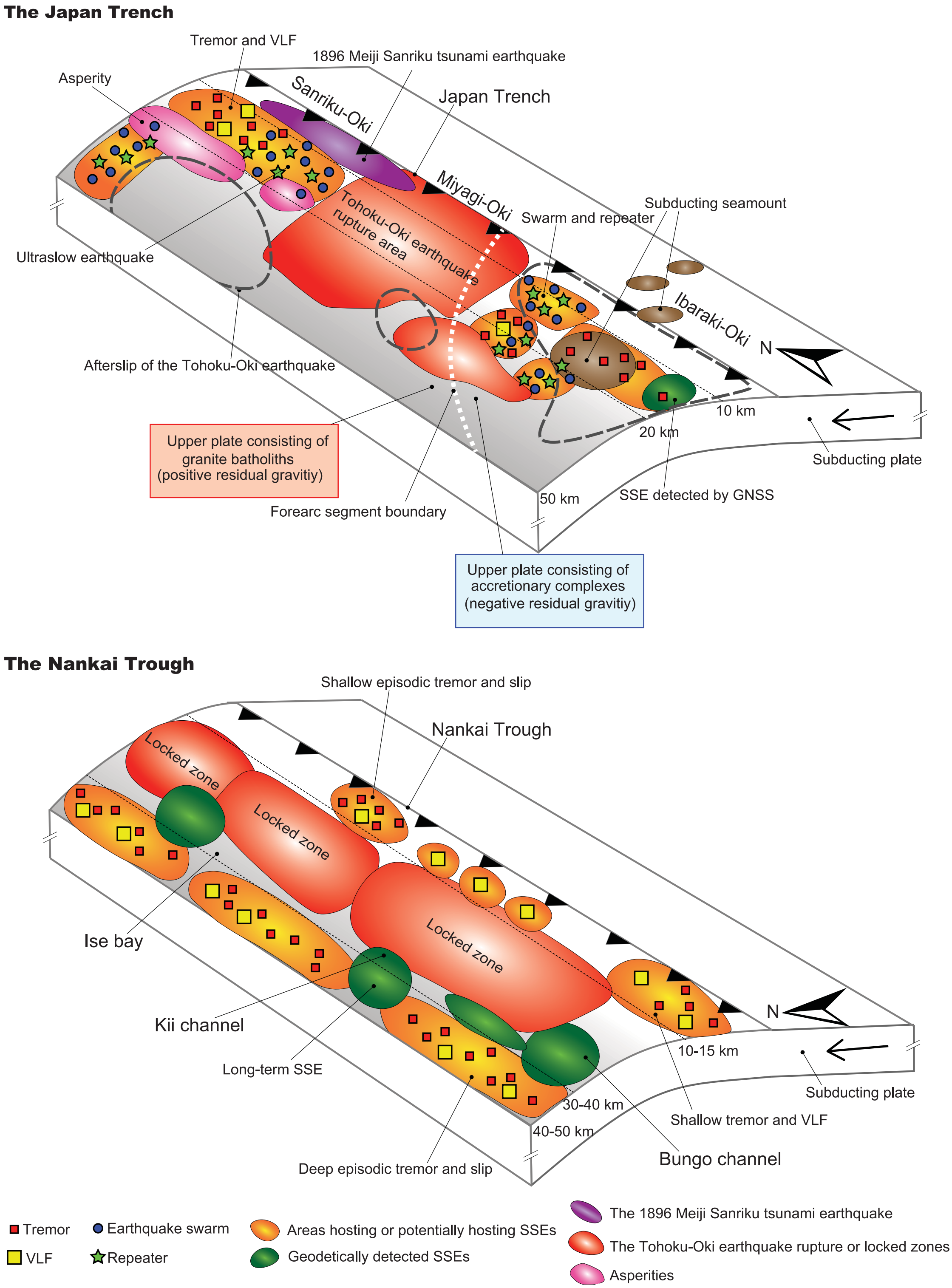

Fig. 4. Schematic views of the slow earthquake activity and structural heterogeneity in the Japan Trench and Nankai Trough. Red and yellow squares denote tectonic tremors and VLFs, respectively. Green stars and blue circles indicate repeaters and earthquake swarms, respectively. The orange regions are interpreted to host or potentially host SSEs accompanied by tremors, VLFs, repeaters, and/or earthquake swarms. The green regions denote geodetically detected SSEs. The purple region is the rupture area of the 1896 Meiji Sanriku tsunami earthquake (*22*) in the Japan Trench. The red regions indicate the coseismic rupture area of the 2011 M_w 9.0 Tohoku-Oki earthquake in the Japan Trench and locked zones in the Nankai Trough. The pink regions indicate the asperities (*33*). The brown regions are subducting seamounts. The dashed dark gray lines denote the afterslip areas of the Tohoku-Oki earthquake in the Japan Trench. The white dashed line indicates the forearc segment boundary (*24*) in the Japan Trench. Note that the slab geometries are simplified. The schematic view of the Nankai Trough is adapted from (*11*).

results suggest frequent occurrence of slow earthquakes in these two segments (Fig. 3, B and C).

This slow earthquake segmentation correlates with the along-strike structural heterogeneity of the Japan Trench (*24*–*26*) (Fig. 4). Tremors, VLFs, and background swarms in the southern segment are located in an area that possesses low *P*-wave velocity and negative residual gravity anomalies, whereas the central segment is characterized by high *P*-wave velocity and positive residual gravity anomalies (*24*, *26*) (fig. S3). High *P*-wave velocity and positive residual gravity anomalies in the southern segment (36°N and 142°E) correspond to a subducting seamount (*25*), where high tremor activity is also observed (fig. S2C). Residual gravity observations help to determine the forearc geological segment boundary (*24*) (Figs. 3 and 4). At this boundary, the density of the rocks overlying the megathrust abruptly increases from south to north. This boundary was suggested to control the rupture extent of the Tohoku-Oki earthquake (*24*). We observed a clear contrast in slow earthquake activity across this boundary. Similar to the southern segment, the source area of the 1989 and 1992 ultraslow earthquakes (*21*) in the northern segment corresponds to a low–*P*-wave velocity anomaly (fig. S3A), although tremors are distributed in both low– and high–*P*-wave velocity anomalies.

We propose that the along-strike structural heterogeneity of the Japan Trench results in different slip behaviors of the three segments, leading to differences in slow earthquake activity, which were clearly demonstrated by homogeneous near-field observation of the S-net (*13*). The low–*P*-wave velocity anomalies in the southern and northern segments may indicate more pore fluids on the megathrust, whereas the central segment is associated with less pore fluid (*26*). Furthermore, the subducting seamount in the southern segment is thought to entrain fluid-rich sediments (*25*). We found these ideas to be consistent with our observations because abundant fluids are one of the possible causes of slow earthquakes and fault creep (*27*). Different upper plate lithologies also exist between the southern and central segments, consisting of accretionary complexes and granitic batholiths, respectively (*24*) (Fig. 4). A simple interpretation is that these variations in pore fluids and lithology yield heterogeneous frictional properties on the megathrust, leading to differences in the slip behavior of the three segments. However, both frictional sliding and ductile deformation of the fault zone, such as pressure-solution creep (fluid-assisted diffusive mass transfer), might play important roles in the generation of slow earthquakes (*27*, *28*). In addition, along-strike variations of subducted sediments and bathymetric features on the incoming Pacific Plate (*29*) might also influence frictional sliding and/or ductile deformation of the plate interface. In the northern and central segments, reflection surveys (*29*) imaged a wedge-shaped sedimentary unit on the plate interface, which diminishes at depths greater than 10 to 13 km. In contrast, in the southern segment, a channel-like sedimentary unit extends further downdip. The incoming seafloor off the northern and central segments is characterized by horst-graben structures, whereas the seafloor off the southern segment is very rugged because of seamounts (Fig. 3A).

Furthermore, the differences in the slip behavior among the three segments might have impeded the rupture propagation of the Tohoku-Oki earthquake. Under the rate-and-state dependent friction framework (*30*), SSEs are often modeled as sliding of a fault patch whose nucleation size is larger than the patch size (*31*), or whose frictional behavior transitions from velocity-weakening to velocity-strengthening as the slip velocity increases (*32*). In these models, the fault patch hosting SSEs can impede the rupture propagation of adjacent earthquakes and host their afterslip (*31*), which is consistent with our observations in the southern and northern segments. In addition, we compared our slow earthquake distribution with coseismic slip areas (asperities) of $M_w \geq 7$ interplate earthquakes (*33*) (fig. S4). We found that the slow earthquake distribution is complementary to the asperity distribution, especially in the northern segment. The asperities are located downdip of the tremor-prone area and the source area of the ultraslow earthquakes. This further supports the hypothesis that areas hosting frequent slow earthquakes impede earthquake rupture propagation.

The slow earthquake activity in the Japan Trench differs considerably from that in the well-studied Nankai Trough (*11*) (Fig. 4). The slip behavior of the megathrust in Nankai transitions from shallow slow earthquakes to megathrust earthquakes to deep slow earthquakes in the downdip direction, and is relatively uniform along strike. In contrast, that in the Japan Trench substantially varies not only in the dip but also in the strike direction. Along-strike segmentation of slow earthquakes and a M_w 9–class megathrust earthquake as in the Japan Trench (Fig. 4) is not known in other subduction zones. The along-dip transition also differs between the Japan Trench and the Nankai Trough. In the south central part of the southern segment, the slip behavior transitions from a tremor-prone area to a swarm-prone area and the coseismic rupture of the Tohoku earthquake (Fig. 4). Deep tremors have not been detected in the Japan Trench. These differences in the along-dip transition might be caused by slab temperature contrast (i.e., a young, warm slab in Nankai versus an old, cold slab in the Japan Trench) and resulting differences in fault zone rheology (*34*). The proximity between tectonic tremors and earthquake swarms is also a feature of the Japan Trench distinct from Nankai. They occur at similar depth ranges (Fig. 4 and fig. S2). It is unclear what physical conditions favor earthquake swarms instead of tremors. However, we noticed that tremors around 36°N and 142°E are located on a subducting seamount, whereas nearby earthquake swarms (36.2°N and 141.9°E) are concentrated downdip of the seamount (fig. S2C). Fracturing of the upper plate resulting from subduction of the seamount (*28*) might be related to the generation of tectonic tremors in the Japan Trench, although tremors around 36.7°N and 40°N are not associated with known subducting seamounts (fig. S2, B and C). In addition, substantial differences between these two subduction zones in terms of relative plate velocity, slab dip angle, tectonic accretion and erosion, sediment thickness, and bathymetric features on the incoming plate (*28*, *35*) might also cause the differences in the slow and megathrust earthquake activity (Fig. 4). The detailed slow earthquake distribution that we mapped provides essential information on heterogeneous frictional properties and fault zone rheology of the megathrust, which in turn provides a potential constraint on the rupture extent of megathrust earthquakes.

REFERENCES AND NOTES

1. S. Ide, G. C. Beroza, D. R. Shelly, T. Uchide, *Nature* **447**, 76–79 (2007).
2. Y. Ito *et al.*, *Tectonophysics* **600**, 14–26 (2013).
3. S. Katakami *et al.*, *J. Geophys. Res.* **123**, 9676–9688 (2018).
4. S. Ruiz *et al.*, *Science* **345**, 1165–1169 (2014).
5. T. H. Dixon *et al.*, *Proc. Natl. Acad. Sci. U.S.A.* **111**, 17039–17044 (2014).
6. F. Rolandone *et al.*, *Sci. Adv.* **4**, eaao6596 (2018).
7. T. Matsuzawa, Y. Asano, K. Obara, *Geophys. Res. Lett.* **42**, 4318–4325 (2015).
8. N. Uchida, A. Hasegawa, T. Matsuzawa, T. Igarashi, *Tectonophysics* **385**, 1–15 (2004).
9. T. Nishikawa, S. Ide, *J. Geophys. Res.* **123**, 7950–7968 (2018).
10. N. Uchida, T. Iinuma, R. M. Nadeau, R. Bürgmann, R. Hino, *Science* **351**, 488–492 (2016).
11. K. Obara, A. Kato, *Science* **353**, 253–257 (2016).
12. National Research Institute for Earth Science and Disaster Resilience, NIED S-net (2019); doi:10.17598/nied.0007.
13. See supplementary materials.
14. S. Tanaka, T. Matsuzawa, Y. Asano, *Geophys. Res. Lett.* **46**, 5217–5224 (2019).
15. K. Ohta *et al.*, *Geophys. Res. Lett.* **46**, 4591–4598 (2019).
16. K. Obara, *Science* **296**, 1679–1681 (2002).
17. T. Iinuma *et al.*, *J. Geophys. Res.* **117**, B07409 (2012).
18. Y. Asano, K. Obara, Y. Ito, *Earth Planets Space* **60**, 871–875 (2008).
19. Y. Ito, K. Obara, K. Shiomi, S. Sekine, H. Hirose, *Science* **315**, 503–506 (2007).
20. T. Iinuma *et al.*, *Nat. Commun.* **7**, 13506 (2016).
21. I. Kawasaki, Y. Asai, Y. Tamura, *Tectonophysics* **330**, 267–283 (2001).
22. Y. Tanioka, K. Sataka, *Geophys. Res. Lett.* **23**, 1549–1552 (1996).
23. T. Nishimura *et al.*, *Geophys. J. Int.* **157**, 901–916 (2004).
24. D. Bassett, D. T. Sandwell, Y. Fialko, A. B. Watts, *Nature* **531**, 92–96 (2016).
25. K. Mochizuki, T. Yamada, M. Shinohara, Y. Yamanaka, T. Kanazawa, *Science* **321**, 1194–1197 (2008).
26. X. Liu, D. Zhao, *Sci. Adv.* **4**, eaat4396 (2018).
27. R. Bürgmann, *Earth Planet. Sci. Lett.* **495**, 112–134 (2018).
28. K. Wang, S. L. Bilek, *Tectonophysics* **610**, 1–24 (2014).
29. T. Tsuru *et al.*, *J. Geophys. Res.* **107**, 2357 (2002).
30. J. H. Dieterich, *J. Geophys. Res.* **84**, 2161–2168 (1979).
31. N. Kato, *J. Geophys. Res.* **109**, B12306 (2004).
32. B. Shibazaki, T. Shimamoto, *Geophys. J. Int.* **171**, 191–205 (2007).
33. Y. Yamanaka, M. Kikuchi, *J. Geophys. Res.* **109**, B07307 (2004).
34. X. Gao, K. Wang, *Nature* **543**, 416–419 (2017).
35. P. Clift, P. Vannucchi, *Rev. Geophys.* **42**, RG2001 (2004).
36. National Research Institute for Earth Science and Disaster Resilience, NIED F-net (2019); doi:10.17598/nied.0005.
37. S. Ide, H. Aochi, *Tectonophysics* **600**, 1–13 (2013).
38. J. Nakajima, F. Hirose, A. Hasegawa, *J. Geophys. Res.* **114**, B08309 (2009).
39. W. H. F. Smith, D. T. Sandwell, *Science* **277**, 1956–1962 (1997).

ACKNOWLEDGMENTS

We thank D. Zhao and S. Ohyanagi for comments. We thank F. Hirose for providing the slab model. **Funding:** Supported by JSPS KAKENHI (18J01056, 16H06477, 15K05260, 16K05536, 16H02219, and 17H05418). **Author contributions:** T. Nishikawa detected the earthquake swarms and wrote the manuscript. S.I. and K.O. detected the tectonic tremors. T.M. detected the very low frequency earthquakes. N.U. detected the repeating earthquakes. T. Nishimura analyzed the GNSS data. All authors discussed the results and commented on the manuscript. **Competing interests:** The authors declare no competing interests. **Data and materials availability:** The datasets generated during this study are included in the supplementary materials. The S-net (*12*) and F-net (*36*) waveform data were provided by NIED. The earthquake catalog used in this study was provided by JMA (www.data.jma.go.jp/svd/eqev/data/bulletin/index_e.html). The GNSS RINEX data were provided by Geospatial Information Authority of Japan (http://terras.gsi.go.jp) and Japan Coast Guard (www1.kaiho.mlit.go.jp/KOHO/dataservice/htdoc1.htm). The coseismic slip and afterslip distribution of the Tohoku-Oki earthquake are from (*17*) and (*20*), respectively. The slab model of the Pacific Plate is based on (*37*) for the entire Japan Trench and on (*38*) for the section adjacent to the Kanto district (www.mri-jma.go.jp/Dep/sv/2ken/fhirose/ja/PlateData.html). The topographic data are from (*39*) (https://topex.ucsd.edu/marine_topo/). The figures were prepared using Generic Mapping Tools (http://gmt.soest.hawaii.edu/).

SUPPLEMENTARY MATERIALS

science.sciencemag.org/content/365/6455/808/suppl/DC1
Materials and Methods
Figs. S1 to S10
References (*40*–*58*)

3 April 2019; accepted 11 July 2019
10.1126/science.aax5618

Science

The slow earthquake spectrum in the Japan Trench illuminated by the S-net seafloor observatories

T. Nishikawa, T. Matsuzawa, K. Ohta, N. Uchida, T. Nishimura and S. Ide

Science **365** (6455), 808-813.
DOI: 10.1126/science.aax5618

Slow earthquake segmentation
The Japan Trench is responsible for disastrous megathrust earthquakes like the 2011 Tohoku-Oki quake. Nishikawa *et al.* used new observations from the S-net ocean-bottom seismic network to map slow earthquakes—disturbances that do not cause ground shaking—along the Japan Trench (see the Perspective by Houston). They found that the area that ruptured during the 2011 quake was bounded by areas that have large numbers of slow earthquakes. A segmentation likely caused the 2011 rupture to cease, an observation that is important for assessing risk from future major earthquakes.
Science, this issue p. 808; see also p. 750

Science (print ISSN 0036-8075; online ISSN 1095-9203) is published by the American Association for the Advancement of Science, 1200 New York Avenue NW, Washington, DC 20005. The title *Science* is a registered trademark of AAAS.